https://doi.org/10.5194/acp-2020-544
Preprint. Discussion started: 30 July 2020

Atmospheric Chemistry and Physics Discussions

Mapping the drivers of formaldehyde (HCHO) variability from 2015−2019 over eastern China: insights from FTIR observation and GEOS-Chem model simulation

Youwen Sun [1)], Hao Yin [1, 3)], Cheng Liu [2, 3, 8, 9, 1)*], Lin Zhang [4)*], Yuan Cheng [5)*], Mathias Palm [6)], Justus Notholt [6)], Xiao Lu [7)], Corinne Vigouroux [10)], Bo Zheng [11)], Wei Wang [1)], Nicholas Jones [12)], Changong Shan [1)], Yuan, Tian [13)], Qihou Hu [1)], and Jianguo Liu [1)]

(1 *Key Laboratory of Environmental Optics and Technology, Anhui Institute of Optics and Fine Mechanics, HFIPS, Chinese Academy of Sciences, Hefei 230031, China*)
(2 *Center for Excellence in Regional Atmospheric Environment, Institute of Urban Environment, Chinese Academy of Sciences, Xiamen, 361021, China*)
(3 *Department of Precision Machinery and Precision Instrumentation, University of Science and Technology of China, Hefei, 230026, China*)
(4 *Laboratory for Climate and Ocean–Atmosphere Studies, Department of Atmospheric and Oceanic Sciences, School of Physics, Peking University, Beijing 100871, China*)
(5 *State Key Laboratory of Urban Water Resource and Environment, School of Environment, Harbin Institute of Technology, Harbin 150090, China*)
(6 *Institute of Environmental Physics, University of Bremen, P. O. Box 330440, 28334 Bremen, Germany*)
(7 *School of Engineering and Applied Sciences, Harvard University, Cambridge, MA 02138, USA*)
(8 *Key Laboratory of Precision Scientific Instrumentation of Anhui Higher Education Institutes, University of Science and Technology of China, Hefei, 230026, China*)
(9 *Anhui Province Key Laboratory of Polar Environment and Global Change, University of Science and Technology of China, Hefei, 230026, China*)
(10 *Royal Belgian Institute for Space Aeronomy (BIRA-IASB), Brussels, Belgium*)
(11 *Laboratoire des Sciences du Climat et de l'Environnement, CEA-CNRS-UVSQ, UMR8212, Gif-sur-Yvette, France*)
(12 *School of Chemistry, University of Wollongong, Northfields Ave, Wollongong, NSW, 2522, Australia*)
(13 *Anhui University Institutes of Physical Science and Information Technology, Hefei 230601, China*)
Correspondence: Cheng Liu (chliu81@ustc.edu.cn), Lin Zhang (zhanglg@pku.edu.cn) and Yuan Cheng (ycheng@hit.edu.cn)

Abstract:

The major air pollutant emissions have decreased and the overall air quality has substantially improved across China in recent years as a consequence of active clean air policies for mitigating severe air pollution problems. As key precursors of formaldehyde (HCHO) and ozone (O_3), the volatile organic compounds (VOCs) in China are still increasing because current clean air policies lack mitigation measures for VOCs. In this study, we mapped the drivers of HCHO variability over eastern China using ground-based high-resolution Fourier transform infrared (FTIR) spectrometry and GEOS-Chem model simulation. Diurnal, seasonal, and interannual variability of HCHO over eastern China was investigated and hydroxyl (OH) radical production from HCHO was evaluated. The relative contributions of emitted and photochemical sources to the observed HCHO were

https://doi.org/10.5194/acp-2020-544
Preprint. Discussion started: 30 July 2020

Atmospheric Chemistry and Physics Discussions

analysed by using ground level carbon monoxide (CO) and O_x (O_3 + nitrogen oxide (NO_2)) as tracers for emitted and photochemical HCHO, respectively. Contributions of various emission sectors and geographical transport to the observed HCHO summertime enhancements were determined by using a GEOS-Chem tagged-tracer simulation. The tropospheric HCHO volume mixing ratio (VMR) reached a maximum monthly mean value of (1.1 ± 0.27) ppbv in July and a minimum monthly mean value of (0.4 ± 0.11) ppbv in January. The tropospheric HCHO VMR time series from 2015 − 2019 shows a positive trend of (1.43 ± 0.14)% per yr. The photochemical HCHO is the dominant source of atmospheric HCHO over eastern China for most of the year (68.1%). In the studied years, the HCHO photolysis was an important source of OH radical over eastern China during all sunlight hours of both summer and winter days. The anthropogenic emissions (fossil fuel + biofuel emissions) accounted for 31.96% and the natural emissions (biomass burning + biogenic) accounted for 48.75% of HCHO summertime enhancements. The observed HCHO summertime enhancements were largely attributed to the emissions within China (76.92%), where eastern China dominated the contribution (46.24%). The increased trend in HCHO in recent years was largely attributed to the increase in the HCHO precursors such as CH_4 and nonmethane VOCs (NMVOCs). This study can provide an evaluation of recent VOC emissions and regional photochemical capacity in China. In addition, this study is also important for regulatory and control purposes and will help to improve urban air quality and contribute to the formation of new Chinese clean air policies in the future.

1 Introduction

Formaldehyde (HCHO) is one of the most critical tropospheric pollutants, which not only directly threatens human health but also plays a significant role in atmospheric photochemical reactions (Franco et al., 2015; Jones et al., 2009; Notholt et al., 1992; Notholt et al., 2000; Vigouroux et al., 2009). Indeed, the chemistry of HCHO is common to virtually all mechanisms of tropospheric chemistry (Chapter 6, Seinfeld and Pandis, 2016). Furthermore, the observation of HCHO variability allows us to constrain volatile organic compound (VOC) emissions and improve current understanding of the complex degradation mechanisms of VOCs (Gao et al., 2018; Viatte et al., 2014; Vigouroux et al., 2018).

Natural sources such as biomass burning and biogenic emissions, and anthropogenic sources such as vehicle exhausts, industrial emissions, and coal combustions can emit HCHO directly into the atmosphere (Albrecht et al., 2002; Holzinger et al., 1999). The emitted HCHO is mainly attributed to incomplete combustion and is closely associated with the emissions of benzene ($C_9H_{12}O$), toluene (C_7H_8), or carbon monoxide (CO) (Friedfeld et al., 2002; Garcia et al. 2006; Ma et al., 2016). In addition, photochemical formation of HCHO has been identified from the atmospheric oxidation of methane (CH_4) and numerous nonmethane VOCs (NMVOCs), which are closely associated with the formation of ozone (O_3) or O_x (O_3 + nitrogen dioxide (NO_2)) or glyoxal (CHOCHO) (Chapter 6, Seinfeld and Pandis, 2016; Friedfeld et al., 2002; Garcia et al. 2006; Zhang et al., 2020). As a result, the relative contribution of emitted and photochemical sources to atmospheric HCHO can be estimated via a linear multiple regression analysis method that aims at reproducing the time series of observed HCHO from a linear combination of the time series of CO (or $C_9H_{12}O$ or C_7H_8) and O_3 (or O_x or CHOCHO) as tracers for emitted and photochemical HCHO, respectively (Friedfeld et al., 2002; Garcia et al., 2006; Hong et al., 2018; Li et al., 2010; Lui et al., 2017; Ma et al., 2016; Su et al., 2019). The separation between emitted and photochemical sources of HCHO is important for improving the air quality in megacities (Garcia et al., 2006).

https://doi.org/10.5194/acp-2020-544
Preprint. Discussion started: 30 July 2020

Atmospheric Chemistry and Physics Discussions

By using the CO – O_3 tracer pair, Friedfeld et al. (2002), Li et al. (2010), Lui et al. (2017), and Su et al. (2019) analysed the relative contribution of emitted and photochemical sources to atmospheric HCHO in Houston in summer 2000, Beijing during the 2008 Olympic Games, Hongkong between winter 2012 and autumn 2013, and the Yangtze River Delta (YRD) in eastern China from 2014−2017, respectively. By using the CO – O_x tracer pair, Hong et al. (2018) estimated the contribution of direct emissions and photochemical formation to atmospheric HCHO along the Yangtze River, China during winter 2015. By using the CO – CHOCHO tracer pair, Garcia et al. (2006) analysed different sources of HCHO in Mexico City in spring 2003. By using the combination of $C_9H_{12}O$ and C_7H_8 as tracers of sources related to petrochemical industries, CO as the tracer of combustion processes including flares and vehicle exhaust, and O_3 as the tracer of photochemical formation, Ma et al. (2016) separated different sources of HCHO in Nanjing, China in spring 2015.

In the aforementioned studies, all gases in Friedfeld et al. (2002), Garcia et al. (2006), Li et al. (2010), Lui et al. (2017), and Ma et al. (2016) were based on ground level measurements using either differential optical absorption spectroscopy (DOAS), Fourier transform infrared spectroscopy (FTIR), non-dispersive infrared spectrometry (NDIR), tunable diode laser absorption spectroscopy (TDLAS), the 2, 4-dinitrophenylhydrazine (DNPH) method, or proton transfer reaction mass spectrometry (PTR-MS). The time series of CO and O_3 or O_x (O_3 + NO_2) in Hong et al. (2018) and Su et al. (2018) are from ground level measurements using either electrochemical gas sensors, DOAS, or the NDIR technique, while the time series of HCHO in Hong et al. (2018) and Su et al. (2018) are from tropospheric vertical column densities (VCDs) using ship-based multi-axis DOAS (MAX-DOAS) and the ozone mapping and profiler suite (OMPS) onboard the Suomi National Polar-orbiting Partnership (Suomi-NPP) satellite, respectively. Tropospheric HCHO column measurements were used as representative of near-surface conditions because the HCHO has a vertical distribution that is heavily weighted toward the lower troposphere over polluted areas.

Previous studies have often concentrated on the separation between emitted and photochemical sources of HCHO, while contributions of different emission sectors and geographical transport were not mentioned or only analysed qualitatively by using the back-trajectories analysis technique. Improved knowledge of the contributions of different emission sectors and geographical transport to HCHO variability is significant for improving the understanding of the HCHO production regime, and further, for regulatory and control purposes (Molina and Molina, 2002; Surl et al., 2018). In this study, the drivers of HCHO variability over eastern China were mapped using ground-based high-resolution FTIR spectrometry and GEOS-Chem model simulation. Diurnal, seasonal, and interannual variability of HCHO over eastern China was investigated and hydroxyl (OH) radical production from HCHO was evaluated. In addition to separation between emitted and photochemical sources, contributions of different emission sectors and geographical transport to the observed HCHO summertime enhancement were also investigated.

China has implemented a series of active clean air policies in recent years to mitigate severe air pollution problems. Therefore, the emissions of major air pollutants have decreased, and the overall air quality has substantially improved (Sun et al., 2019; Zhang et al., 2019; Zheng et al., 2018). However, current clean air policies lack mitigation measures for VOCs, which are key precursors of HCHO and O_3 (Lu et al., 2018; Zheng et al., 2018). The increasing trend in O_3 in recent years in China was largely attributed to the increase in VOCs (Lu et al., 2019). Multi-year time series of ground-based FTIR measurements of HCHO in this study provide an evaluation of

https://doi.org/10.5194/acp-2020-544
Preprint. Discussion started: 30 July 2020

Atmospheric Chemistry and Physics Discussions

recent VOC emissions in China. The degradation of HCHO provides a large source of OH radicals, which play a significant role in atmospheric photochemical reactions (Chapter 6, Seinfeld and Pandis, 2016). The OH radical production rate from HCHO photolysis estimated in this study provides an evaluation of regional photochemical capacity over eastern China. In addition, source separation and attribution for HCHO variability in this study can contribute to the formation of new Chinese clean air policies in the future.

The next section describes the FTIR tropospheric HCHO VMR data, the ground level CO and O_x (O_3 + NO_2) VMR data, the 3rd regression model used to determine seasonal and interannual variability of HCHO, the linear regression model used for source separation, and the GEOS-Chem tagged-tracer simulation used for source attribution. Section 3 reports the results for model evaluation, HCHO variability on different time scales, source separation, and OH radical production rates from HCHO photolysis over eastern China. Section 4 reports the results for source attribution using GEOS-Chem tagged-tracer simulation. Conclusions are presented in Section 5.

2 Methods and data

2.1 FTIR tropospheric HCHO VMRs

The tropospheric column-averaged VMRs of HCHO were retrieved from direct solar absorption spectra recorded with a ground-based high-resolution FTIR spectrometer at Hefei (117°10′E, 31°54′N) over eastern China (Tian et al., 2018; Sun et al., 2018). The FTIR routine observations at Hefei alternately acquired a suite of solar spectra per day. The number of HCHO daily measurements from 2015−2019 varied from 1−17 with an average of six. The SFIT4 version 0.9.4.4 algorithm was used in the profile retrieval, and the retrieval settings were prescribed from a harmonisation project described in Vigouroux et al. (2018). Four micro-windows (MWs) were used: two strong lines within 2778–2782 cm^{-1} and two weak lines within 2763–2766 cm^{-1} (Vigouroux et al., 2018). All spectroscopic absorption parameters were based on the atm16 line list from the compilation of Geoffrey Toon (Vigouroux et al., 2018). The *a priori* profiles of temperature, pressure, and H_2O were interpolated from the National Centers for Environmental Protection (NCEP) 6-hourly reanalysis data and the *a priori* profiles of other gases were from the Whole-Atmosphere Community Climate Model (WACCM) simulation. The profiles of CH_4 and O_3 and columns of HDO and N_2O were simultaneously retrieved in addition to the HCHO profile for minimising the cross interference. The diagonal elements of the *a priori* profile covariance matrix $\mathbf{S}_a$ and the measurement noise covariance matrix $\mathbf{S}_\varepsilon$ were set to standard deviation of the WACCM special run and the inverse square of the signal-to-noise ratio (SNR) of each spectrum, respectively (De Maziere et al., 2018; Viatte et al., 2014). The non-diagonal elements of both $\mathbf{S}_a$ and $\mathbf{S}_\varepsilon$ were set to zero. The measured instrument line shape (ILS) was employed in the retrieval (Hase et al., 2012; Sun et al., 2018).

We only considered the retrievals with total degrees of freedom (DOFS) larger than 0.7 and root-mean-square (RMS) of fitting residuals less than 2%. Fig. 1 shows the averaging kernels, cumulative sum of DOFS, and VMR of randomly selected HCHO retrievals. The vertical distribution of the FTIR HCHO retrieval is heavily weighted toward the lower troposphere. In the following analysis, HCHO VMR averaged between the surface and 10 km altitude is referred to as tropospheric HCHO VMR. This selected layer is fully within the tropopause height at Hefei throughout the four seasons (Sun et al., 2020). The selected layer corresponds to 1.0 ± 0.1 (1σ) of DOFS and 10.2 ± 1.3 (1σ)% of retrieval error (Sun et al., 2018).

https://doi.org/10.5194/acp-2020-544
Preprint. Discussion started: 30 July 2020

Atmospheric Chemistry and Physics Discussions

2.2 Ground level CO and O_x (O_3 + NO_2)

The ground level in situ CO, O_3, and NO_2 time series were provided by the China National Environmental Monitoring Center (CNEMC) network maintained by the Chinese Ministry of Ecology and Environment (http://www.cnemc.cn/en/, last access: 22 March 2020).The CNEMC network has monitored six ground level air pollutants (including CO, O_3, NO_2, SO_2, PM_{10}, and $PM_{2.5}$) in nationwide sites in mainland China since 2013, and by 2019, it was extended to more than 2000 sites in 454 cities. The datasets have been used in many studies to evaluate local air quality over China (Gao et al., 2018; Hong et al., 2018; Hu et al., 2017; Li et al., 2018; Lu et al., 2018; Shen et al., 2019; Su et al., 2019). The measurements taken at the nearest CNEMC site, which is approximately 700 m away from the FTIR site, were used in this study. A filtering criterion following that of Su et al. (2019) and Lu et al. (2019) was applied to remove unreliable hourly measurements.

2.3 Regression model for seasonal and interannual variability

The seasonality and interannual trend of tropospheric HCHO VMRs from 2015−2019 over eastern China were evaluated using a bootstrap resampling method following that of Gardiner et al. (2008). Gardiner et al. (2008)'s method has been used by many studies to estimate the variability of atmospheric composition on different time scales (including Gardiner et al., 2008; Jones et al., 2009; Sun et al., 2018; Sun et al., 2020; Tian et al., 2017; Viatte et al., 2014; Vigouroux et al., 2015; Vigouroux et al., 2018; Zeng et al., 2012). The following regression model, Model-1 ($Y_{hcho}^{mod1}(t)$) was applied to fit the FTIR tropospheric HCHO VMR time series $Y_{hcho}^{meas}(t)$:

$$Y_{hcho}^{meas}(t) = Y_{hcho}^{mod1}(t) + \varepsilon(t) \quad (1)$$

$$Y_{hcho}^{mod1}(t) = A_0 + A_1 t + A_2 \cos\left(\frac{2\pi t}{365}\right) + A_3 \sin\left(\frac{2\pi t}{365}\right) + A_4 \cos\left(\frac{4\pi t}{365}\right) + A_5 \sin\left(\frac{4\pi t}{365}\right) \quad (2)$$

$$d\% = \frac{Y_{hcho}^{meas}(t) - Y_{hcho}^{mod1}(t)}{Y_{hcho}^{mod1}(t)} \times 100 \quad (3)$$

where A_0 is the intercept, A_1 is the annual growth rate, and A_1/A_0 is the interannual trend discussed below. The A_2–A_5 parameters describe the seasonal cycle, t is the measurement time elapsed since 2015, and $\varepsilon(t)$ represents the residuals between the measurements and the fitting model. In this study, daily mean time series were used to lower the residuals and to improve the fitting correlation. Furthermore, fractional differences of FTIR tropospheric HCHO VMR time series relative to their seasonal mean values represented by $Y_{hcho}^{mod1}(t)$ were also calculated in equation (3) to analyse seasonal enhancements.

2.4 Regression model for source separation

The emitted and photochemical HCHO over eastern China were separated by using ground level CO and O_x (O_3 + NO_2) as tracers, respectively. The methodology in this study follows that of Friedfeld et al. (2002), which has been used extensively in source separation for atmospheric HCHO (including Friedfeld et al., 2002; Garcia et al., 2006; Hong et al., 2018; Li et al., 1994; Li et al., 2010, Lui et al., 2017; Ma et al., 2016, Su et al., 2019; Wang et al., 2015). Over polluted atmosphere, O_3 reacts with NO emitted from vehicle exhaust to form NO_2. In this case, O_x (O_3 + NO_2) is in principle a better surrogate of photochemical processes as it also accounts for titrated O_3 (Garcia et al., 2006; Li et al., 1994). Therefore, this study uses O_x as a tracer for photochemical HCHO. A linear regression model was used to establish a link among the time series of HCHO, CO, and O_x (Garcia

https://doi.org/10.5194/acp-2020-544
Preprint. Discussion started: 30 July 2020

Atmospheric Chemistry and Physics Discussions

et al., 2006). The observed HCHO $Y_{hcho}^{meas}(t)$ can be reproduced by the following linear regression model Model-2 ($Y_{hcho}^{mod2}(t)$):

$$Y_{hcho}^{meas}(t) = Y_{hcho}^{mod2}(t) + \varepsilon(t) \quad (4)$$

$$Y_{hcho}^{mod2}(t) = \alpha_0 + \alpha_1 \times Y_{co}^{meas}(t) + \alpha_2 \times Y_{ox}^{meas}(t) \quad (5)$$

where α_0, α_1, and α_2 represent the fitted coefficients; and $\varepsilon(t)$ is the fitting residual, which is assumed to be independent with a constant variance and a mean of zero (Garcia et al., 2006). $Y_{co}^{meas}(t)$ and $Y_{ox}^{meas}(t)$ are ground level VMR time series of CO and O_x, respectively. The relative contributions of emitted (R_e), photochemical (R_p), and background (R_b) sources to the observed HCHO can be calculated by (Friedfeld et al., 2002; Garcia et al., 2006; Hong et al., 2018; Li et al. 2010, Lui et al. 2017; Ma et al., 2016; Su et al., 2019; Wang et al., 2015):

$$R_e = \frac{\alpha_1 \times Y_{co}^{meas}(t)}{\alpha_0 + \alpha_1 \times Y_{co}^{meas}(t) + \alpha_2 \times Y_{ox}^{meas}(t)} \quad (6)$$

$$R_p = \frac{\alpha_2 \times Y_{ox}^{meas}(t)}{\alpha_0 + \alpha_1 \times Y_{co}^{meas}(t) + \alpha_2 \times Y_{ox}^{meas}(t)} \quad (7)$$

$$R_b = \frac{\alpha_0}{\alpha_0 + \alpha_1 \times Y_{co}^{meas}(t) + \alpha_2 \times Y_{ox}^{meas}(t)} \quad (8)$$

To compare the results, the regression analysis in Garcia et al. (2006) was run using subsets of data, which comprise a comparable number of data points for each considered time period. By dividing the data into several periods of interest, it is possible to lower the residual and improve the fitting correlation (Garcia et al., 2006). For short-term time series of HCHO, the background α_0, which is neither classified as emitted or photochemical contributions, can be fixed at an empirical constant level to initialise the linear regression model (Garcia et al., 2006; Hong et al., 2018; Ma et al., 2016; Su et al., 2019; Wang et al., 2015;). This empirical background level was derived from statistics of previous studies in the studied region or estimated from a chemical model simulation by turning off all emissions (Hong et al., 2018; Su et al., 2019). For the multi-year time series of HCHO in this study, all measurements were grouped by month, and the empirical background level of previous studies in the YRD region was used, coupled with a 3rd Fourier series to reconcile the seasonal difference in HCHO background.

According to the ground level measurements of HCHO in the YRD region by Ma et al. (2016) and Wang et al. (2015), the background level of HCHO near the surface was approximately 1 ppbv in springtime. This ground level (1 ppbv) was converted into a tropospheric averaged level by scaling the concurrent retrieved HCHO profile. As a result, the fitting process was initiated by assigning the background with a 3rd Fourier series with an amplitude of 0.22 ppbv.

2.5 GEOS-Chem tagged-tracer simulation for source attribution

The drivers of the observed HCHO variability over eastern China were determined by using the GEOS-Chem chemical transport model version 12.2.1 in a tagged mode (Bey et al., 2001; http://geos-chem.org, last access on 14 February 2020). GEOS-Chem model implements a universal tropospheric-stratospheric Chemistry (UCX) mechanism (Eastham et al., 2014). The model configurations used in this study are summarised in Table 1 and were designed as follows.

(i) To analyse the contribution of various emission sectors, each individual emission inventory was turned off to evaluate the change of the simulation in the presence of all other emission inventories. Thus, the relative contribution of each emission sector was estimated as the relative difference between the GEOS-Chem simulation in the presence and absence of the tagged emission

https://doi.org/10.5194/acp-2020-544
Preprint. Discussion started: 30 July 2020

inventory. Four such tagged simulations were conducted by turning off (1) fossil fuel emissions (including emissions from agriculture, industry, power plant, residential, and transport), (2) biogenic emissions, (3) biomass burning emissions, and (4) biofuel emissions (Table 1). The combination of fossil fuel and biofuel emissions is referred to as anthropogenic emission, and the combination of biogenic and biomass burning emissions is referred to as natural emission.

(ii) To analyse the contribution of different geographical regions, emission inventories within each geographical region were turned off to assess the change of the simulation in the presence of emission inventories outside the tagged geographical region. Thus, the relative contribution of each geographical region was estimated as the relative difference between the GEOS-Chem simulation in the presence and absence of emission inventories within the tagged geographical region. Six such tagged simulations were conducted by turning off all anthropogenic and natural emissions within six geographical regions (Table 1). The geographical regions are shown in Fig. 2 and the resulting regional definitions are summarised in Table 2.

All simulations were performed in a standard GEOS-Chem full-chemistry mode with a horizontal resolution of 2° × 2.5°. All simulations were initialised for one year (July 2014−July 2015) to remove the influence of the initial conditions. All simulations were driven by the Goddard Earth Observing System-Forward Processing (GEOS-FP) meteorological fields at a horizontal resolution of 2◦ × 2.5◦ degraded from their native resolution of 0.25° × 0.3125°. The GEOS-Chem model outputs 72 vertical layers of HCHO VMR concentration ranging from the surface to 0.01 hPa at a temporal resolution of 1 h. Only the HCHO simulations from 2015−2019 between the surface and 10 km altitude were considered for the grid box containing Hefei (31.52°–32.11°N by 116.53°–118.02°E).

The global fossil fuel and biofuel emissions were from the Community Emissions Data System (CEDS) inventory (Hoesly et al., 2018), which overwrites regional emissions over Asia with the MIX inventory (Li et al., 2017; Lu et al., 2019; Zheng et al., 2018). In particular, the latest Chinese anthropogenic emissions for 2017 from the Multi-resolution Emission Inventory for China (MEIC; http://www.meicmodel.org, last access: 14 April 2020) were implemented (Lu et al., 2019; Zheng et al., 2018). Global biomass burning emissions were from the Global Fire Emissions Database version 4 (GFED4) inventory (Giglio et al., 2013). Biogenic emissions were from the Model of Emissions of Gases and Aerosols from Nature (MEGAN version 2.1) inventory (Guenther et al., 2012), and soil NO_x emissions were calculated following the method of Hudman et al. (2010, 2012). The photolysis rates were obtained from the FAST-JX v7.0 photolysis scheme (Bian and Prather, 2002). Dry deposition was calculated by the resistance-in-series algorithm (Wesely, 1989; Zhang et al., 2001), and wet deposition followed that of Liu et al. (2001).

3 Tropospheric HCHO VMR time series by FTIR and GEOS-Chem model

3.1 Model evaluation

The GEOS-Chem model was used to evaluate the diurnal HCHO variability and contributions of various emission sectors and geographical transport to the observed HCHO summertime enhancement. Model evaluation is an essential procedure in advance of subsequent studies. The FTIR tropospheric HCHO VMR time series was compared to the GEOS-Chem BASE simulation to investigate the chemical model performance for the specifics of polluted regions over eastern China (Table 1). As the vertical resolution of GEOS-Chem profile is different from the FTIR measurements, a smoothing correction was applied for the GEOS-Chem profiles. First, the GEOS-

https://doi.org/10.5194/acp-2020-544
Preprint. Discussion started: 30 July 2020

Atmospheric Chemistry and Physics Discussions

Chem HCHO profiles were interpolated to the FTIR altitude grid to ensure a common altitude grid. The interpolated profiles were then smoothed by the concurrent FTIR averaging kernels and *a priori* profiles (Rodgers, 2000; Rodgers and Connor, 2003). The GEOS-Chem tropospheric HCHO VMRs were calculated subsequently from the smoothed profiles. Finally, the GEOS-Chem tropospheric HCHO VMRs were compared with the FTIR data.

Fig. 3 (a) shows the tropospheric HCHO VMR time series comparison between the FTIR observation and the smoothed GEOS-Chem model simulation from 2015−2019 over eastern China. Generally, the GEOS-Chem and FTIR tropospheric HCHO VMRs are in good agreement with a correlation coefficient (r) of 0.88. The measured features in terms of daily variability, seasonality, and interannual variability can be reproduced by GEOS-Chem simulations. The averaged difference between GEOS-Chem and FTIR data (GEOS-Chem minus FTIR) was (0.05 ± 0.2) ppbv (2.6 ± 10.4)%, which is within the FTIR uncertainty budget. As a result, GEOS-Chem can simulate the trace gas concentrations and variations for the heavily polluted regions in China. Therefore, GEOS-Chem for the subsequent studies can be used with confidence.

The largest GEOS-Chem vs. FTIR differences tended to occur in the trough and peak of the measurements. These differences were attributed mainly to a coarse spatial resolution of GEOS-Chem, which homogenises HCHO concentration over a larger coverage area. The Hefei site is in a densely populated and industrialised area in eastern China. The regional difference in HCHO concentration levels could aggravate the inhomogeneity within the selected GEOS-Chem coverage area, and thus exaggerate the difference. Additionally, the difference in the temporal resolution of GEOS-Chem and FTIR (± 30 min) could also cause inconsistencies due to the exceedingly high variability of atmospheric HCHO.

3.2 Diurnal, seasonal, and interannual variability

Because the FTIR measurements cannot provide a full diurnal cycle (see Section 2.1), the GEOS-Chem model BASE simulation has been used to study the diurnal cycle of HCHO. As seen from Fig. 4 (a), tropospheric HCHO VMR usually increases over time in the morning, reaches the maximum in late morning (DJF) or around midday (MAM/JJA/SON), and then decreases during the rest of the day. The hourly variations in the night-time [after 18:00 local time (LT)] are larger than those in the daytime for all seasons except winter, which shows a larger hourly variation in daytime. On average, the daytime hourly variation spanned a large range of -33.7−34.6%, depending on the season and measurement time.

In comparison, ground level O_x VMR usually increased over time in the morning, reaching a maximum in the afternoon, and then decreasing during the rest of the day [Fig. 4 (b)]. The hourly variations in O_x in the daytime (before 18:00 LT) were larger than those in the night-time for all seasons. The typical diurnal variations in ground level CO VMR [Fig. 4(c)] were significantly different from those of HCHO and are quite dependent on the combined influence of regional vehicle exhausts, industrial emissions, and coal combustions. Generally, large variations in CO were observed during rush hours (8:00 to 11:00 LT in the morning and 16:00 to 19:00 LT in the afternoon) in all seasons.

Tropospheric HCHO VMR daily mean time series comparison between FTIR observations and the regression model $Y_{hcho}^{mod1}(t)$ from 2015−2019 over eastern China is shown in Fig. 3 (b). Generally, the regression model $Y_{hcho}^{mod1}(t)$ can capture the features in terms of seasonality and interannual variability measured by the FTIR in a good agreement with a correlation coefficient (r)

https://doi.org/10.5194/acp-2020-544
Preprint. Discussion started: 30 July 2020

Atmospheric Chemistry and Physics Discussions

of 0.81. Therefore, the model $Y_{hcho}^{mod1}(t)$ is used to evaluate the seasonal and interannual variability in HCHO.

Tropospheric HCHO VMR roughly increases over time for the first half of the year and decreases over time for the second half of the year (Fig. 5). The tropospheric HCHO VMR reached a maximum monthly mean value of (1.1 ± 0.27) ppbv in July and a minimum monthly mean value of (0.4 ± 0.11) ppbv in January. Tropospheric HCHO VMRs in July were on average 1.75 times higher than those in January. As commonly observed, the seasonal enhancement spanned a large range of -50.0%−60.0% depending on the season and measurement time [Fig. 5 (b)]. The tropospheric HCHO VMR time series from 2015−2019 showed a positive trend of (1.43 ± 0.14)% per yr [Fig. 3 (b)]. This positive trend in HCHO concentration over China observed by ground-based FTIR was in agreement with the positive trends observed by the spaceborne Ozone Monitoring Instrument (OMI) from 2004−2014 by De Smedt et al. (2015) and from 2005−2017 by Zhang et al. (2019). Many air pollutants, such as NO_2, sulphur dioxide (SO_2), particulate matter 2.5 ($PM_{2.5}$), particulate matter 10 (PM_{10}), CO, black carbon (BC), and organic carbon (OC), showed negative trends in recent years as a consequence of active clean air policies enforced by the Chinese government since 2013 to mitigate severe air pollution problems. However, current clean air policies lack mitigation measures for VOCs. The opposite trend in HCHO concentration may urge an action plan involving VOC emissions control in the future.

3.3 Separation between emitted and photochemical sources

The tropospheric HCHO VMR time series comparison between FTIR observation and the regression model $Y_{hcho}^{mod2}(t)$ from 2015−2019 over eastern China is shown in Fig. 3 (c). Seasonal variabilities of absolute and relative contributions of emitted, photochemical, and background sources to the observed HCHO VMR are shown in Fig. 6. Generally, the regression model $Y_{hcho}^{mod2}(t)$ can capture the daily variability, seasonality, and interannual variability measured by FTIR with a correlation coefficient (r) of 0.83. Therefore, the authors are confident that model $Y_{hcho}^{mod2}(t)$ can be used for the subsequent studies of source separation.

Statistical modelling results for relative contributions of different sources to the observed HCHO VMRs from 2015−2019 over eastern China are listed in Table 3. The contributions of emitted and photochemical sources spanned a large range of values throughout the year; however, the contribution of the background source was roughly a constant value. Depending on measurement times and season, the contribution from emitted sources varied from 14.0%−58.0%, and contribution from photochemical sources varied from 20%−82%. On average, the contributions of emitted, photochemical, and background sources to the observed HCHO VMRs from 2015−2019 were 29.0 ± 19.2%, 49.2 ± 18.5%, and 21.8 ± 6.1%, respectively.

All measurements were further separated into emission-dominated or photochemical-dominated measurements according to a larger contribution to the observed HCHO VMR (Table 3). Generally, photochemical HCHO is the dominant source of atmospheric HCHO over eastern China for most of the year (68.1%). The largest contrast between photochemical and emitted in terms of domination fraction occurs in the afternoon (after 12:00 a.m. LT) in JJA/SON season when the photochemistry of VOCs is active for both HCHO and O_3 formation.

3.4 Hydroxyl radical (OH) production from HCHO

Photolysis plays a significant role in the degradation of HCHO and one of its two photo

https://doi.org/10.5194/acp-2020-544
Preprint. Discussion started: 30 July 2020

Atmospheric Chemistry and Physics Discussions

dissociative paths provides a large source of OH radicals. The photolysis pathways of HCHO to form the OH radical are summarised as follows (Chapter 6, Seinfeld and Pandis, 2016):

$$HCHO + h\nu \rightarrow H + HCO \ (\lambda \leq 370\ \text{nm}) \rightarrow H_2 + CO \quad (9)$$

$$H + O_2 \rightarrow HO_2 \quad (10)$$

$$HCO + O_2 \rightarrow HO_2 + CO \quad (11)$$

$$HO_2 + NO \rightarrow OH + NO_2 \quad (12)$$

In air, the photolysis of HCHO first generates a hydroperoxyl (HO_2) radical at wavelengths below 370 nm. Then, HO_2 rapidly reacts with nitric oxide (NO) to generate the OH radical, and subsequently affects the oxidative capacity of the atmosphere (Possanzini et al., 2002; Volkamer et al., 2010). Under steady-state conditions, the total OH radical production rate from the photolysis of HCHO through the above chain of reactions is:

$$\frac{p[OH]_{HCHO}}{dt} = 2J_a[HCHO] \quad (13)$$

where [HCHO] is the concentration of HCHO and J_a is the photolysis constant of reaction (9). In comparison, applying steady state to reactions (14)–(16),

$$O_3 + h\nu \rightarrow O_2 + O(1D) \quad (14)$$

$$O(1D) + M_{air} \rightarrow O(3P) + M_{air} \quad (15)$$

$$O(1D) + H_2O \rightarrow 2OH \quad (16)$$

the total OH radical production rate from O_3 is given by (Chapter 6, Seinfeld and Pandis, 2016),

$$\frac{p[OH]_{O_3}}{dt} = 2J_c\frac{k_e}{k_d}\frac{[O_3][H_2O]}{[M_{air}]} \quad (17)$$

where $[O_3]$, $[H_2O]$, and $[M_{air}]$ are the concentrations of O_3, H_2O, and air, respectively; J_c is the photolysis constant of reaction (14); and k_d and k_e are the reaction rate coefficients for (15) and (16), respectively. In this study, photolysis rate constants for HCHO and O_3 were available from the GEOS-Chem simulation, and the reaction rate coefficients were calculated according to a well-known procedure (Table B1; Seinfeld and Pandis, 2016). Surface H_2O concentrations were available from an in situ cavity ring-down spectroscopy (CRDS) analyser (G2401-m, Picarro, Inc., USA) (Tian et al., 2018). For the atmosphere N_2/O_2 mixture at 298 K, the values of k_d and k_e are 2.9×10^{-11} and 2.2×10^{-10} cm^3 $molecule^{-1}s^{-1}$, respectively. The air concentration $[M_{air}]$ is 0.99 molecules cm^{-3} (Chapter 6, Seinfeld and Pandis, 2016). The concentrations of HCHO and O_3 were based on FTIR observations and the CNEMC network, respectively. To reconcile the difference between the ground level concentration and tropospheric column-averaged concentration, the FTIR tropospheric HCHO VMRs were converted to ground level VMRs by scaling the respective retrieved profiles.

The total OH radical production rates from the photolysis of HCHO and O_3 from 2015−2019 over eastern China calculated via equations (13) and (17) are shown in Fig. 7. For both gases, the OH radical production rates in summertime are higher than those in wintertime. Generally, OH radical production rates from the photolysis of HCHO are comparable with those from the photolysis of O_3 in all seasons. In wintertime when the concentrations in O_3 and H_2O are low, or when emitted sources dominate the HCHO measurements, OH radical production rates from HCHO photolysis are higher than those from O_3 photolysis. In other seasons, when the concentrations in O_3 and H_2O are high, or when photochemical sources dominate the HCHO measurements, OH radical production rates from HCHO photolysis are lower than those from O_3 photolysis. On average, the OH production rate from O_3 photolysis is 6.1% higher than that of HCHO photolysis. The results clearly indicate that HCHO photolysis was by far an important source of OH radicals over eastern

https://doi.org/10.5194/acp-2020-544
Preprint. Discussion started: 30 July 2020

Atmospheric Chemistry and Physics Discussions

China during all sunlight hours of both summer and winter days.

4 Source attribution by GEOS-Chem tagged-tracer simulation

4.1 Emission sector contribution to HCHO enhancement

In this study, the summertime HCHO observations are selected, which generally show the maximum seasonal enhancement throughout the year, to analyse the contribution of each emission sector. Fig. 8 explores the absolute and relative contributions of fossil fuel, biogenic, biomass burning, and biofuel emissions to the observed HCHO summertime enhancement from 2015−2019 over eastern China. The GEOS-Chem simulations were decreased by 0.37, 0.59, 0.02, and 0.02 ppbv in the absence of fossil fuel, biogenic, biomass burning, and biofuel emission inventories, respectively, which correspond to 30.27, 47.39, 1.36, and 1.69% of relative contribution to the observed HCHO summertime enhancement, respectively. The anthropogenic emissions accounted for 31.96% and the natural emissions account for 48.75% of HCHO summertime enhancement. The remaining contribution was calculated as the difference between the BASE simulation and the sum of all anthropogenic and natural contributions and was 0.21 ppbv (19.29%). This contribution can be regarded as the atmospheric HCHO background, which is similar to the background contribution deduced in Section 3.3.

The statistics of the GEOS-Chem emission inventories show that the anthropogenic CO emissions reduced by 27% and the NMVOCs emissions increased by 11% in China from 2010−2017 (Lu et al., 2019; Zheng et al., 2018). The biogenic isoprene and CH_4 emissions increased by 6.5% and 1%, respectively, over eastern China in 2017 relative to 2016 (Lu et al., 2019). Sun et al. (2020) observed a decrease in the number of fires in China since 2015 when the Chinese government started to ban crop residue burning events throughout China. Because the emission of HCHO is positively related to the emission of CO, a decrease in CO either from anthropogenic or natural sources could also indicate a decrease in emitted HCHO. In contrast, the increase in the HCHO precursors such as CH_4 and NMVOCs could cause an increase in photochemical HCHO. An overall increase in HCHO from 2015−2019 indicates that the decrease in emitted HCHO was overwhelmed by the increase in HCHO precursor emissions from growing activities.

4.2 Geographical region contribution to HCHO enhancement

The summertime HCHO observations were selected to analyse the contribution of each geographical region. Fig. 9 explores the absolute and relative contributions of emissions in ER, CR, NR, WR, SR, and ROW regions to the observed HCHO summertime enhancement from 2015−2019 over eastern China. Geographical definitions of these regions are summarised in Table 2. The GEOS-Chem simulations were decreased by 0.57, 0.2, 0.03, 0.02, 0.12, and 0.26 ppbv in the absence of the emissions in ER, CR, NR, WR, SR, and ROW regions, respectively, which correspond to 46.24%, 16.35%, 3.15%, 1.36%, 9.83%, and 23.08% of relative contribution to the observed HCHO summertime enhancement, respectively.

As a short lifetime species (a few hours), the emitted HCHO is heavily weighted toward the direct vicinity of local emission regions. However, HCHO precursors originating from distant areas can be transported to the Hefei site under favourable weather conditions, and thus contribute to photochemical HCHO formation. In addition, the compounds originating either nearby or in distant areas, which affect the chemistry of HCHO or its precursors, could also contribute to photochemical HCHO formation or background. The results show that the observed HCHO summertime

https://doi.org/10.5194/acp-2020-544
Preprint. Discussion started: 30 July 2020

Atmospheric Chemistry and Physics Discussions

enhancement was largely attributed to emissions within China (76.92%), where eastern China dominated the contribution (46.24%). Near the observation site, emissions over the ER region dominated both the emitted and photochemical HCHO. Emissions outside the ER region mainly contributed to the photochemical or background HCHO because of long-distance transport.

The emissions in western China are typically lower than those in rest of China because of lower population and industries in the region (Lu et al., 2019; Zheng et al., 2018). The strong easterly and the south-westerly flows prevail in the lower troposphere during the summer Asian monsoon, including the South Asian summer monsoon and East Asian summer monsoon (Liu et al., 2003; Wu et al., 2012). For contributions from outside the ER region, the lowest contribution of the WR region to the observed HCHO summertime enhancement is largely attributed to the lowest HCHO precursor emissions in this region. A smaller contribution of the NR region to HCHO summertime enhancement in comparison with SR and CR regions is mainly attributed to less air masses that originated in northern China during the summer Asian monsoon.

5 Concluding remarks

China has implemented a series of active clean air policies in recent years to mitigate severe air pollution problems. Therefore, the emissions of major air pollutants have decreased and the overall air quality across China has substantially improved. However, the VOC emissions, which are key precursors of HCHO and ozone, are still increasing because the current clean air policies in China lack mitigation measures for VOCs.

This study mapped the drivers of the observed variability in HCHO over eastern China using ground-based high-resolution FTIR spectrometry and GEOS-Chem model simulation. The tropospheric HCHO VMR reached a maximum monthly mean value of (1.1 ± 0.27) ppbv in July and a minimum monthly mean value of (0.4 ± 0.11) ppbv in January. Tropospheric HCHO VMRs in July were on average 1.75 times higher than those in January. The tropospheric HCHO VMR time series from 2015−2019 showed a positive trend of (1.43 ± 0.14)% per yr. The relative contributions of emitted and photochemical sources to the observed HCHO were analysed using ground level CO and O_x (O_3 + NO_2) as tracers for emitted and photochemical HCHO, respectively. On average, the contributions of emitted, photochemical, and background sources to the observed HCHO VMRs from 2015−2019 were 29.0 ± 19.2%, 49.2 ± 18.5%, and 21.8 ± 6.1%, respectively. The photochemical HCHO was the dominant source of atmospheric HCHO over eastern China for most of the year (68.1%). In the studied years, total OH radical production rates from the photolysis of HCHO and O_3 were comparable. The HCHO photolysis was by far an important source of OH radicals over eastern China during all sunlight hours of both summer and winter days.

Contributions of different emission sectors and geographical transport to the observed HCHO were determined by using GEOS-Chem model to evaluate the relative change of the simulation in absence of the tagged emission inventory. The results showed that anthropogenic emissions accounted for 31.96% and natural emissions accounted for 48.75% of HCHO summertime enhancement. The observed HCHO summertime enhancements were largely attributed to the emissions within China (76.92%), where eastern China dominated the contribution. The increased trend in the HCHO in recent years in China was largely attributed to the increase in HCHO precursors such as CH_4 and NMVOCs.

This study can provide an evaluation of recent VOC emissions and regional photochemical capacity in China. In addition, this study is important for regulatory and control purposes and should

https://doi.org/10.5194/acp-2020-544
Preprint. Discussion started: 30 July 2020

help to improve urban air quality and contributes to the formation of new Chinese clean air policies in the future.

Data availability. The FTIR HCHO measurements and GEOS-Chem tagged-tracer simulations in this study are available on request.

Author contributions. YS conceived the concept and prepared the paper with input from all coauthors. HY carried out the GEOS-Chem simulations. The rest authors contributed to this work via provide refined data or constructive comments.

Competing interests. The authors declare that they have no conflict of interest.

Acknowledgements. This work is jointly supported by the National High Technology Research and Development Program of China (No.2019YFC0214802, No.2017YFC0210002, 2018YFC0213201, 2019YFC0214702, and 2016YFC0200404), the National Science Foundation of China (No. 41575021, No. 51778596, No. 41977184, and No.41775025), the Major Projects of High Resolution Earth Observation Systems of National Science and Technology(05-Y30B01-9001-19/20-3), the Sino-German Mobility programme (M-0036), and Anhui Province Natural Science Foundation of China (No. 2008085QD180). The processing and post processing environment for SFIT4 are provided by National Center for Atmospheric Research (NCAR), Boulder, Colorado, USA. The NDACC network is acknowledged for supplying the SFIT software. The LINEFIT code is provided by Frank Hase, Karlsruhe Institute of Technology (KIT), Institute for Meteorology and Climate Research (IMK-ASF), Germany. We thank the senate of Bremen, Germany for support. We thank the FTIR group at university of Wollongong, Australia for help in setting up and operating the FTIR spectrometer at Hefei. We thank the FTIR group at Royal Belgian Institute for Space Aeronomy (BIRA-IASB), Belgium for providing harmonized HCHO retrieval setup. We thank the GEOS-Chem team for the support and Tsinghua University, China for providing the latest MEIC inventory.

References

Albrecht, T. , Notholt, J. , Wolke, R. , Solberg, S. , Dye, C. , and Malberg, H.: Variations of CH_2O and C_2H_2 determined from ground-based ftir measurements and comparison with model results. advances in space research, 29, 1713-1718, 2002.

Bey, I., Jacob, D. J., Yantosca, R. M., Logan, J. A., Field, B. D., Fiore, A. M., Li, Q., Liu, H. Y., Mickley, L. J., and Schultz, M. G.: Global modeling of tropospheric chemistry with assimilated meteorology: Model description and evaluation, J. Geophys. Res., 106, 23073–23095, https://doi.org/10.1029/2001jd000807, 2001.

Bian, H. and Prather, M. J.: Fast-J2: Accurate Simulation of Stratospheric Photolysis in Global Chemical Models, J. Atmos. Chem., 41, 281–296, https://doi.org/10.1023/a:1014980619462, 2002.

De Smedt, I., Stavrakou, T., Hendrick, F., Danckaert, T., Vlemmix, T., Pinardi, G., Theys, N., Lerot, C., Gielen, C., Vigouroux, C., Hermans, C., Fayt, C., Veefkind, P., Müller, J.-F., and Van Roozendael, M.: Diurnal, seasonal and long-term variations of global formaldehyde columns inferred from combined OMI and GOME-2 observations, Atmos. Chem. Phys., 15, 12519–12545, https://doi.org/10.5194/acp-15-12519-2015, 2015.

Eastham, S., D. , Weisenstein, D. K., Barrett S., R., H.: Development and evaluation of the unified

https://doi.org/10.5194/acp-2020-544
Preprint. Discussion started: 30 July 2020

tropospheric-stratospheric chemistry extension (UCX) for the global chemistry-transport model GEOS-Chem, Atmos. Environ., 89,52-63, 2014.

Fisher, J. A., Murray, L., Jones, D. B. A., and Deutscher, N. M.: Improved method for linear carbon monoxide simulation and source attribution in atmospheric chemistry models illustrated using GEOS-Chem v9, Geosci. Model Dev., 10, 4129–4144, https://doi.org/10.5194/gmd-10-4129-2017, 2017.

Friedfeld, S., Fraser, M., Ensor, K., et al.: Statistical analysis of primary and secondary atmopsheric formaldehyde, Atmos. Environ.,36, 477–4775, 2002.

Franco, B., Hendrick, F., Van Roozendael, M., Müller, J.-F., Stavrakou, T., Marais, E. A., Bovy, B., Bader, W., Fayt, C., Hermans, C., Lejeune, B., Pinardi, G., Servais, C., and Mahieu, E.: Retrievals of formaldehyde from ground-based FTIR and MAX-DOAS observations at the Jungfraujoch station and comparisons with GEOS-Chem and IMAGES model simulations, Atmos. Meas. Tech., 8, 1733-1756, https://doi.org/10.5194/amt-8-1733-2015, 2015.

Gardiner, T., Forbes, A., de Mazière, M., Vigouroux, C., Mahieu, E., Demoulin, P., Velazco, V., Notholt, J., Blumenstock, T., Hase, F., Kramer, I., Sussmann, R., Stremme, W., Mellqvist, J., Strandberg, A., Ellingsen, K., and Gauss, M.: Trend analysis of greenhouse gases over Europe measured by a network of ground-based remote FTIR instruments, Atmos Chem Phys, 8, 6719-6727, 2008.

Giglio, L., Randerson, J. T., and van der Werf, G. R.: Analysis of daily, monthly, and annual burned area using the fourth-generation global fire emissions database (GFED4), Journal of Geophysical Research: Biogeosciences, 118, 317–328, https://doi.org/10.1002/jgrg.20042, 2013.

Garcia, A. R., Volkamer, R., Molina, L. T., Molina, M. J., Samuelson, J., Mellqvist, J., Galle, B., Herndon, S. C., and Kolb, C. E.: Separation of emitted and photochemical formaldehyde in Mexico City using a statistical analysis and a new pair of gas-phase tracers, Atmos. Chem. Phys., 6, 4545–4557, https://doi.org/10.5194/acp-6-4545-2006, 2006.

Guenther, A. B., Jiang, X., Heald, C. L., Sakulyanontvittaya, T., Duhl, T., Emmons, L. K., and Wang, X.: The Model of Emissions of Gases and Aerosols from Nature version 2.1 (MEGAN2.1): An extended and updated framework for modeling biogenic emissions, Geosci. Model Dev., 5, 1471–1492, https://doi.org/10.5194/gmd-5-1471-2012, 2012.

Giuseppe, F. D., Rémy, S., Pappenberger, F., and Wetterhall, F.: Using the Fire Weather Index (FWI) to improve the estimation of fire emissions from fire radiative power (FRP) observations, Atmos. Chem. Phys., 18, 5359–5370, https://doi.org/10.5194/acp-18-5359-2018, 2018.

Gao, M., Beig, G., Song, S., Zhang, H., Hu, J., Ying, Q., Liang, F., Liu, Y., Wang, H., Lu, X., Zhu, T., Carmichael, G. R., Nielsen, C. P., and McElroy, M. B.: The impact of power generation emissions on ambient PM2.5 pollution and human health in China and India, Environ. Int., 121, 250-259, https://doi.org/10.1016/j.envint.2018.09.015, 2018.

Cao, H., Fu, T. M., Zhang, L., Henze, D. K., Miller, C. C., Lerot, C., Abad, G. G., De Smedt, I., Zhang, Q., van Roozendael, M., Hendrick, F., Chance, K., Li, J., Zheng, J., and Zhao, Y.: Adjoint inversion of Chinese non-methane volatile organic compound emissions using space-based observations of formaldehyde and glyoxal, Atmos. Chem. Phys., 18, 15017–15046, https://doi.org/10.5194/acp-18-15017-2018, 2018.

Hase, F.: Improved instrumental line shape monitoring for the ground-based, high-resolution FTIR spectrometers of the Network for the Detection of Atmospheric Composition Change, Atmos.

https://doi.org/10.5194/acp-2020-544
Preprint. Discussion started: 30 July 2020

Meas. Tech., 5, 603-610,doi:10.5194/amt-5-603-2012, 2012.

Holzinger, R., Warneke, C., Hansel, A., Jordan, A., Lindinger, W., Scharffe, D. H., Schade, G., and Crutzen, P. J.: Biomass burning as a source of formaldehyde, acetaldehyde, methanol, acetone, acetonitrile, and hydrogen cyanide,Geophys.Res.Lett.,26,1161-1164,doi:10.1029/1999gl900156, 1999.

Hong, Q., Liu, C., Chan, K. L., Hu, Q., Xie, Z., Liu, H., Si, F., and Liu, J.: Ship-based MAX-DOAS measurements of tropospheric NO_2, SO_2, and HCHO distribution along the Yangtze River, Atmos. Chem. Phys., 18, 5931–5951, https://doi.org/10.5194/acp-18-5931-2018, 2018.

Hu, J., Li, X., Huang, L., Ying, Q., Zhang, Q., Zhao, B., Wang, S., and Zhang, H.: Ensemble prediction of air quality using the WRF/CMAQ model system for health effect studies in China, Atmos. Chem. Phys., 17, 13103–13118, https://doi.org/10.5194/acp-17-13103-2017, 2017.

Hoesly R. M., Smith S. J., Feng L. Y., Klimont Z., Janssens-Maenhout G., Pitkanen T., Seibert J. J., Vu L., Andres R. J., Bolt R. M., Bond T. C., Dawidowski L., Kholod N., Kurokawa J., Li M., Liu L., Lu Z. F., Moura M. C. P., O'Rourke P. R., and Zhang Q.: Historical (1750-2014) anthropogenic emissions of reactive gases and aerosols from the Community Emissions Data System (CEDS), Geosci. Model Dev., 11, 369-408, 2018.

Hudman, R. C., Russell, A. R., Valin, L. C., and Cohen, R. C.: Interannual variability in soil nitric oxide emissions over the United States as viewed from space, Atmos. Chem. Phys., 10, 9943–9952, https://doi.org/10.5194/acp-10-9943-2010, 2010.

Hudman, R. C., Moore, N. E., Mebust, A. K., Martin, R. V., Russell, A. R., Valin, L. C., and Cohen, R. C.: Steps towards a mechanistic model of global soil nitric oxide emissions: implementation and space based-constraints, Atmos. Chem. Phys., 12, 7779–7795, https://doi.org/10.5194/acp-12-7779-2012, 2012.

Jones, N. B., Riedel, K., Allan, W., Wood, S., Palmer, P. I., Chance, K., and Notholt, J.: Long-term tropospheric formaldehyde concentrations deduced from ground-based fourier transform solar infrared measurements, Atmos. Chem. Phys., 9, 7131–7142, https://doi.org/10.5194/acp-9-7131-2009, 2009.

Li, Y., Shao, M., Lu, S., Chang, C.-C., and Dasgupta, P. K.:Variations and sources of ambient formaldehyde for the 2008 Beijing Olympic games, Atmos. Environ., 44, 2632–2639, https://doi.org/10.1016/j.atmosenv.2010.03.045, 2010.

Li, S., M., Anlauf, K., G., Wiebe, A., Bottenheim, J., W., Estimating primary and secondary production of HCHO in eastern North America based on gas phase measurements and principal component analysis, Geophysical Research Letters, 21, 669-672, https://doi.org/10.1029/94GL00643, 1994.

Li M., Zhang Q., Kurokawa J., Woo J. H., He K. B., Lu Z. F., Ohara T., Song Y., Streets D. G., Carmichael G. R., Cheng Y. F., Hong C. P., Huo H., Jiang X. J., Kang S. C., Liu F., Su H., and Zheng B., :MIX: a mosaic Asian anthropogenic emission inventory under the international collaboration framework of the MICS-Asia and HTAP, Atmos. Chem. Phys. 17, 935-963, 2017.

Li, N., He, Q., Greenberg, J., Guenther, A., Li, J., Cao, J., Wang, J., Liao, H., Wang, Q., and Zhang, Q.: Impacts of biogenic and anthropogenic emissions on summertime ozone formation in the Guanzhong Basin, China, Atmos. Chem. Phys., 18, 7489–7507, https://doi.org/10.5194/acp-18-7489-2018, 2018.

Liu, H., Jacob, D. J., Bey, I., and Yantosca, R. M.: Constraints from 210Pb and 7Be on wet deposition and transport in a global three-dimensional chemical tracer model driven by

https://doi.org/10.5194/acp-2020-544
Preprint. Discussion started: 30 July 2020

assimilated meteorological fields, J. Geophys. Res., 106, 12109–12128, https://doi.org/10.1029/2000jd900839, 2001.

Liu, H., Jacob, D., J., Bey, I., Yantosca, R., M., Duncan, B., N.: Transport pathways for asian pollution outflow over the pacific: interannual and seasonal variations. Journal of Geophysical Research, 108(D20), 8786, 2003.

Lu, X., Hong, J., Zhang, L., Cooper, O. R., Schultz, M. G., Xu, X., Wang, T., Gao, M., Zhao, Y., and Zhang, Y.: Severe Surface Ozone Pollution in China: A Global Perspective, Environ. Sci. Tech. Let., 5, 487–494, https://doi.org/10.1021/acs.estlett.8b00366, 2018.

Lu, X., Zhang, L., Chen, Y., Zhou, M., Zheng, B., Li, K., Liu, Y., Lin, J., Fu, T.-M., and Zhang, Q.: Exploring 2016–2017 surface ozone pollution over China: source contributions and meteorological influences, Atmos. Chem. Phys., 19, 8339–8361, https://doi.org/10.5194/acp-19-8339-2019, 2019.

Lui, K. H., Ho, S. S. H., Louie, P. K. K., Chan, C. S., Lee, S. C., Hu, D., Chan, P. W., Lee, J. C. W., and Ho, K. F.: Seasonal behavior of carbonyls and source characterization of formaldehyde (HCHO) in ambient air, Atmos. Environ., 152, 51–60, https://doi.org/10.1016/j.atmosenv.2016.12.004, 2017.

Martine De Mazière, M., Thompson, A. M., Kurylo, M. J., Wild, J. D., Bernhard, G., Blumenstock, T., Braathen, G. O., Hannigan, J. W., Lambert, J. C., Leblanc, T., Mcgee, T. J., Nedoluha, G., Petropavlovskikh, I., Seckmeyer, G., Simon, P. C., Steinbrecht, W., and Strahan, S. E.: The Network for the Detection of Atmospheric Composition Change (NDACC): history, status and perspectives, Atmos. Chem. Phys., 18, 4935-4964,doi:10.5194/acp-18-4935-2018, 2018.

Ma, Y., Diao, Y., Zhang, B., Wang, W., Ren, X., Yang, D., Wang, M., Shi, X., and Zheng, J.: Detection of formaldehyde emissions from an industrial zone in the Yangtze River Delta region of China using a proton transfer reaction ion-drift chemical ionization mass spectrometer, Atmos. Meas. Tech., 9, 6101–6116, https://doi.org/10.5194/amt-9-6101-2016, 2016.

Molina, L., T. and Molina, M., J.: Air Quality in the Mexico Megacity, Kluwer Academia Publishers, Netherlands, 2002.

Notholt, J., Hjorth, J., Raes, F., and Schrems, O.: Simultaneous long path field measurements of HNO_2, CH_2O and aerosol. Berichte Der Bunsengesellschaft/physical Chemistry Chemical Physics, 96(3), 290-293, 1992.

Notholt, J., Toon, G. C., Rinsland, C. P., Pougatchev, N. S., Jones, N. B., Connor, B. J., Weller, R., Gautrois, M., and Schrems, O.: Latitudinal variations of trace gas concentrations in the free troposphere measured by solar absorption spectroscopy during a ship cruise, J. Geophys. Res. – Atmos., 105, 1337-1349, doi:10.1029/1999jd900940, 2000.

Possanzini, M., Palo, V., D., Cecinato, A.: Sources and photodecomposition of formaldehyde and acetaldehyde in Rome ambient air, Atmos. Environ., 36(19), 3195-3201, 2002.

Rodgers, C. D.: Inverse Methods for Atmospheric Sounding: Theory and Practice, Singapore, 2000.

Rodgers, C. D. and Connor, B. J.: Intercomparison of remote sounding instruments, J. Geophys. Res. – Atmos., 108,4116, https://doi.org/10.1029/2002JD002299, 2003.

Rothman, L. S., Gordon, I. E., Barbe, A., Benner, D. C., Bernath, P. E., Birk, M., Boudon, V., Brown, L. R., Campargue, A., Champion, J. P., Chance, K., Coudert, L. H., Dana, V., Devi, V. M., Fally, S., Flaud, J. M., Gamache, R. R., Goldman, A., Jacquemart, D., Kleiner, I., Lacome, N., Lafferty, W. J., Mandin, J. Y., Massie, S. T., Mikhailenko, S. N., Miller, C. E., Moazzen-Ahmadi, N., Naumenko, O. V., Nikitin, A. V., Orphal, J., Perevalov, V. I., Perrin, A., Predoi-

https://doi.org/10.5194/acp-2020-544
Preprint. Discussion started: 30 July 2020

Cross, A., Rinsland, C. P., Rotger, M., Simeckova, M., Smith, M. A. H., Sung, K., Tashkun, S. A., Tennyson, J., Toth, R. A., Vandaele, A. C., and Vander Auwera, J.: The HITRAN 2008 molecular spectroscopic database,J. Quant. Spectrosc. Ra., 110, 533-572,doi:10.1016/j.jqsrt.2009.02.013, 2009.

Su, W., Liu, C., Hu, Q., Zhao, S., Sun, Y., Wang, W., Zhu, Y., Liu, J., and Kim, J.: Primary and secondary sources of ambient formaldehyde in the Yangtze River Delta based on Ozone Mapping and Profiler Suite (OMPS) observations, Atmos. Chem. Phys., 19, 6717–6736, https://doi.org/10.5194/acp-19-6717-2019, 2019.

Seinfeld, J. H. and Pandis, S. N.: Atmospheric chemistry and physics: from air pollution to climate change, John Wiley & Sons, California, USA, 2016.

Sun, Y. W., Liu, C., Palm, M., Vigouroux, C., Notholt, J., Hui, Q. H., Jones, N., Wang, W., Su, W. J., Zhang, W. Q., Shan, C. G., Tian, Y., Xu, X. W., De Maziere, M., Zhou, M. Q., and Liu, J. G.: Ozone seasonal evolution and photochemical production regime in the polluted troposphere in eastern China derived from high-resolution Fourier transform spectrometry (FTS) observations, Atmos. Chem. Phys., 18, 14569-14583,doi:10.5194/acp-18-14569-2018, 2018a.

Sun, Y. W., Palm, M., Liu, C., Hase, F., Griffith, D., Weinzierl, C., Petri, C., Wang, W., and Notholt, J.: The influence of instrumental line shape degradation on NDACC gas retrievals: total column and profile, Atmos. Meas. Tech., 11, 2879-2896,doi:10.5194/amt-11-2879-2018, 2018b.

Sun, Y., Liu, C., Zhang, L., Palm, M., Notholt, J., Yin, H., Vigouroux, C., Lutsch, E., Wang, W., Shan, C., Blumenstock, T., Nagahama, T., Morino, I., Mahieu, E., Strong, K., Langerock, B., De Mazière, M., Hu, Q., Zhang, H., Petri, C., and Liu, J.: Fourier transform infrared time series of tropospheric HCN in eastern China: seasonality, interannual variability, and source attribution, Atmos. Chem. Phys., 20, 5437–5456, https://doi.org/10.5194/acp-20-5437-2020, 2020.

Surl, L., Palmer, P. I., and González Abad, G.: Which processes drive observed variations of HCHO columns over India?, Atmos. Chem. Phys., 18, 4549–4566, https://doi.org/10.5194/acp-18-4549-2018, 2018.

Shen, L., Jacob, D. J., Liu, X., Huang, G., Li, K., Liao, H., and Wang, T.: An evaluation of the ability of the Ozone Monitoring Instrument (OMI) to observe boundary layer ozone pollution across China: application to 2005–2017 ozone trends, Atmos. Chem. Phys., 19, 6551–6560, https://doi.org/10.5194/acp-19-6551-2019, 2019.

Tian, Y., Sun, Y., Liu, C., Wang, W., Shan, C., Xu, X., and Hu, Q.: Characterisation of methane variability and trends from near-infrared solar spectra over Hefei, China, Atmos. Environ., 173,doi:10.1016/j.atmosenv.2017.11.001, 2017.

Vigouroux, C., Hendrick, F., Stavrakou, T., Dils, B., De Smedt, I., Hermans, C., Merlaud, A., Scolas, F., Senten, C., Vanhaelewyn, G., Fally, S., Carleer, M., Metzger, J., M., Müller, J., F., Van Roozendael, M., and De Mazière, M.: Ground-based FTIR and MAX-DOAS observations of formaldehyde at Réunion Island and comparisons with satellite and model data, Atmos. Chem. Phys., 9, 9523–9544, https://doi.org/10.5194/acp-9-9523-2009,2009.

Vigouroux, C., Blumenstock, T., Coffey, M., Errera, Q., García, O., Jones, N. B., Hannigan, J. W., Hase, F., Liley, B., Mahieu, E., Mellqvist, J., Notholt, J., Palm, M., Persson, G., Schneider, M.,Servais, C., Smale, D., Thölix, L., and De Mazière, M.: Trends of ozone total columns and vertical distribution from FTIR observations at eight NDACC stations around the globe, Atmos.

https://doi.org/10.5194/acp-2020-544
Preprint. Discussion started: 30 July 2020

Chem. Phys., 15, 2915–2933, https://doi.org/10.5194/acp-15-2915-2015, 2015.

Volkamer, R., Sheehy, P., Molina, L. T., and Molina, M. J.: Oxidative capacity of the Mexico City atmosphere – Part 1: A radical source perspective, Atmos. Chem. Phys., 10, 6969–6991, https://doi.org/10.5194/acp-10-6969-2010, 2010.

Viatte, C., Strong, K., Walker, K. A., and Drummond, J. R.: Five years of CO, HCN, C_2H_6, C_2H_2, CH_3OH, HCOOH and H_2CO total columns measured in the Canadian high Arctic, Atmos. Meas. Tech., 7, 1547-1570, https://doi.org/10.5194/amt-7-1547-2014, 2014.

Wang, M., Chen, W., Shao, M., Lu, S., Zeng, L., and Hu, M.: Investigation of carbonyl compound sources at a rural site in the Yangtze River Delta region of China, J. Environ. Sci., 28, 128–136, https://doi.org/10.1016/j.jes.2014.12.001, 2015.

Wang, C., Huang, X., F., Han, Y., Zhu, B., and He, L., Y.: Sources and potential photochemical roles of formaldehyde in an urban atmosphere in South China. J. Geophys. Res. – Atmos., 122, 11,934–11,947.https://doi.org/10.1002/2017JD027266, 2017.

Wesely, M. L.: Parameterization of Surface Resistances to Gaseous Dry Deposition in Regional-Scale Numerical-Models, Atmos. Environ., 23, 1293–1304, https://doi.org/10.1016/0004-6981(89)90153-4, 1989.

Wu, G., Liu, Y., He, B., Bao, Q., Duan, A., and Jin, F.-F.: Thermal controls on the Asian summer monsoon, Sci. Rep., 2, 404, doi:10.1038/srep00404, 2012.

Zhang, L. M., Gong, S. L., Padro, J., and Barrie, L.: A size-segregated particle dry deposition scheme for an atmospheric aerosol module, Atmos. Environ., 35, 549–560, https://doi.org/10.1016/S1352-2310(00)00326-5, 2001.

Zhang, C., Liu, C., Hu, Q., Cai, Z., Su, W., Xia, C., Zhu, Y., Wang, S., and Liu, J.: Satellite UV-Vis spectroscopy: implications for air quality trends and their driving forces in China during 2005–2017, Light: Sci. & Appl., 8, 100, doi:10.1038/s41377-019-0210-6, 2019.

Zhang, C., Liu, C., Chan, K.L., Hu, Q., H., Liu, H. R., Li, B., Xing, C., Z., Tan, W., Zhou, H., J., Si, F., Q., and Liu, J., G.: First observation of tropospheric nitrogen dioxide from the Environmental Trace Gases Monitoring Instrument onboard the GaoFen-5 satellite. Light Sci. & Appl. 9, 66 https://doi.org/10.1038/s41377-020-0306-z, 2020.

Zhang, Q., Zheng, Y., X., Tong, D., Shao, M., Wang, S., X., Zhang, Y., H., Xu, X., D., Wang, J., N., He, H., Liu, W., Q., Ding, Y., H., Lei, Y., Li, J., H., Wang, Z., F., Zhang, X., Y., Wang, Y., S., Cheng, J., Liu, Y., Shi, Q. R., Yan, L., Geng, G. N., Hong, C., P., Li, M., Liu, F., Zheng, B., Cao, J. J., Ding, A., J., Gao, J., Fu, Q., Y., Huo, J., T., Liu, B., X., Liu, Z., R., Yang, F., M., He, K., B., and Hao, J., M.: Drivers of improved PM2.5 air quality in China from 2013 to 2017, Proceedings of the National Academy of Sciences of the United States of America, 116, 24463-24469, 2019.

Zheng, B., Tong, D., Li, M., Liu, F., Hong, C., Geng, G., Li, H., Li, X., Peng, L., Qi, J., Yan, L., Zhang, Y., Zhao, H., Zheng, Y., He, K., and Zhang, Q.: Trends in China's anthropogenic emissions since 2010 as the consequence of clean air actions, Atmos. Chem. Phys., 18, 14095-14111, doi: 10.5194/acp-18-14095-2018, 2018.

Zeng, G., Wood, S. W., Morgenstern, O., Jones, N. B., Robinson, J., and Smale, D.: Trends and variations in CO, C_2H_6, and HCN in the Southern Hemisphere point to the declining anthropogenic emissions of CO and C_2H_6, Atmos Chem Phys, 12, 7543-7555, 10.5194/acp-12-7543-2012, 2012.

https://doi.org/10.5194/acp-2020-544
Preprint. Discussion started: 30 July 2020

Atmospheric Chemistry and Physics Discussions

Tables

Table 1. GEOS-Chem model configurations

Tracer	Abbreviation	Description
None	BASE	Standard full chemistry simulation implemented all anthropogenic and natural emissions at the same time. The BASE simulation is taken as the reference and used for model evaluation
Fossil fuel	noFF	Same as BASE but without global fossil fuel emissions
Biogenic	noBVOC	Same as BASE but without global biogenic emissions
Biomass burning	noBB	Same as BASE but without global biomass burning emissions
Biofuel	noBIOF	Same as BASE but without global biofuel emissions
Western China	noWR	Same as BASE but without anthropogenic and natural emissions within region 1 in Fig. 2
Northern China	noNR	Same as BASE but without anthropogenic and natural emissions within region 2 in Fig. 2
Central China	noCR	Same as BASE but without anthropogenic and natural emissions within region 3 in Fig. 2
Eastern China	noER	Same as BASE but without anthropogenic and natural emissions within region 4 in Fig. 2
Southern China	noSR	Same as BASE but without anthropogenic and natural emissions within region 5 in Fig. 2
Rest of world	noROW	Same as BASE but without anthropogenic and natural emissions within region 6 in Fig. 2

Table 2. Regional definitions of all geographical tracers

Mark	Tracer	Region	Description
1	WR	78.6° E – 103.4° E; 27.6°N - 48.8°N	Covering most of western China and part of neighbouring countries
2	NR	103.4°E – 129.8°E; 34.6°N – 53.5°N	Covering most of northern China and part of neighbouring countries
3	CR	103.4°E – 115.6°E; 27.6°N – 34.6°N	Central China
4	ER	115.6°E – 123.6°E; 21.0°N – 34.6°N	Eastern China
5	SR	98.1°E – 115.6°E; 21.0°N – 27.6°N	Covering most of southern China and part of neighbouring countries
6	ROW	Rest of world	Rest of world

Table 3. Statistical modelling results for contributions of different sources to the observed HCHO VMRs from 2015−2019 over eastern China

Items	Total N (%)	Emission domination N (%)	Photochemical domination N (%)	Background domination N (%)
All	1502 (100%)	480 (31.9%)†	1022 (68.1%)	0 (0)
Before 12:00 (LT)	727 (48.4%)	322 (21.4%)	405 (27.0%)	0 (0)
After 12:00 (LT)	775 (51.6%)	158 (10.5%)	617 (41.1%)	0 (0)
JJA/SON	890 (59.3%)	287 (19.1%)	603 (40.1%)	0 (0)
DJF/MAM	612 (40.7%)	193 (12.8%)	419 (27.9%)	0 (0)
$d\% > 0\%$	717 (47.7%)	273 (18.2%)	444 (29.6%)	0 (0)
$d\% < 0\%$	785 (52.3%)	207 (13.8%)	578 (38.5%)	0 (0)
Contribution	100%	29.0 ± 19.2%††	49.2 ± 18.5%	21.8 ± 6.1%

†There are 480 measurements dominated by emitted source which accounts for 31.9% of all measurements
††The mean contribution of emitted source is 29.0 ± 19.2%.

https://doi.org/10.5194/acp-2020-544
Preprint. Discussion started: 30 July 2020

Atmospheric Chemistry and Physics Discussions

Figures

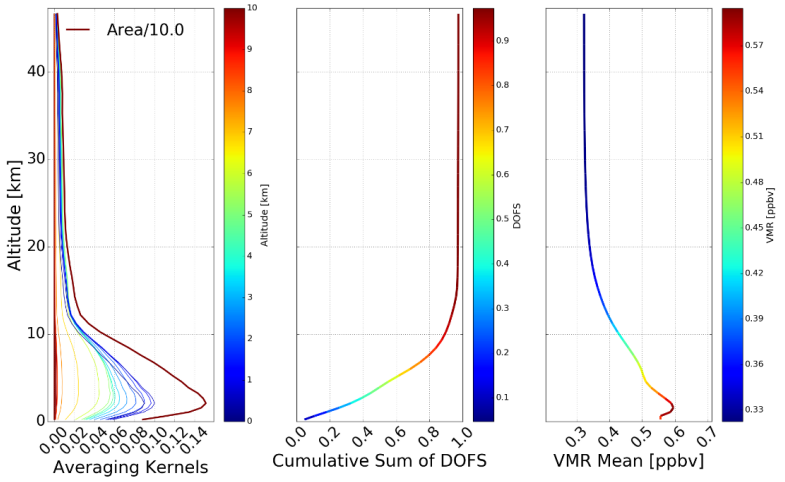

Fig. 1 Averaging kernels, cumulative sum of degrees of freedom (DOFS) and volume mixing ratio (VMR) of randomly selected HCHO retrievals.

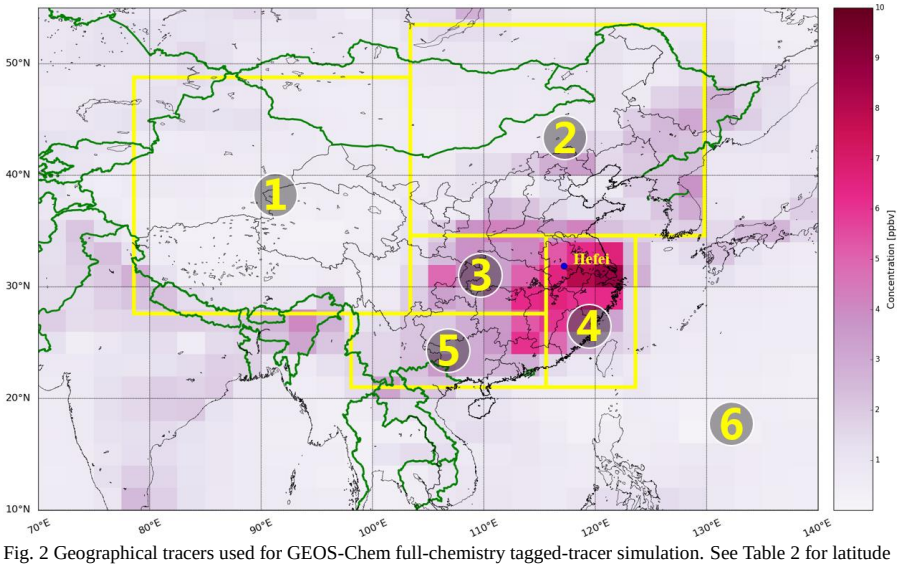

Fig. 2 Geographical tracers used for GEOS-Chem full-chemistry tagged-tracer simulation. See Table 2 for latitude and longitude definitions. GEOS-Chem HCHO simulations on 24 July 2016 were selected for demonstration of summertime enhancement over eastern China.

https://doi.org/10.5194/acp-2020-544
Preprint. Discussion started: 30 July 2020

Atmospheric Chemistry and Physics Discussions

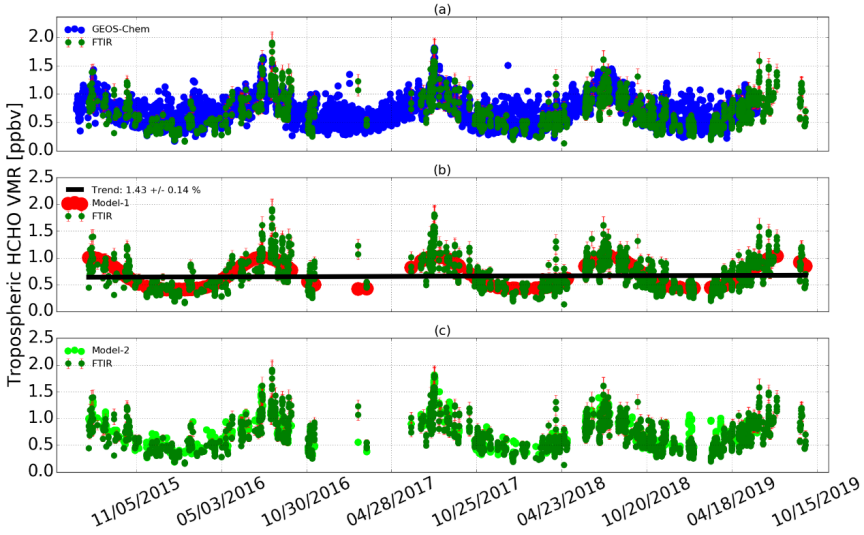

Fig. 3 FTIR time series of tropospheric HCHO VMR from 2015−2019 over eastern China. Concurrent GEOS-Chem model simulations (a) and the fitted results by using the regression model $Y_{hcho}^{mod1}(t)$ (b) (equation (2)) and $Y_{hcho}^{mod2}(t)$ (c) (equation (5)) were also included for comparison. Vertical error bars represent retrieval uncertainties.

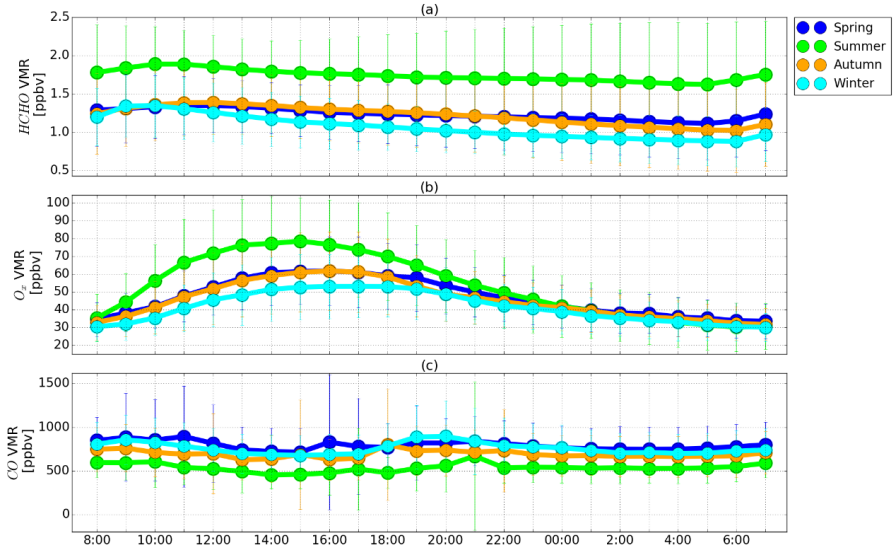

Fig. 4 Diurnal variations of tropospheric HCHO VMR (a), ground level O_x VMR (b), and CO VMR (c) from 2015−2019 over eastern China. Vertical error bars represent 1σ variation within that hour. Tropospheric HCHO VMRs are from GEOS-Chem model, and ground level O_x and CO VMRs are from the CNEMC network.

https://doi.org/10.5194/acp-2020-544
Preprint. Discussion started: 30 July 2020

Atmospheric Chemistry and Physics Discussions

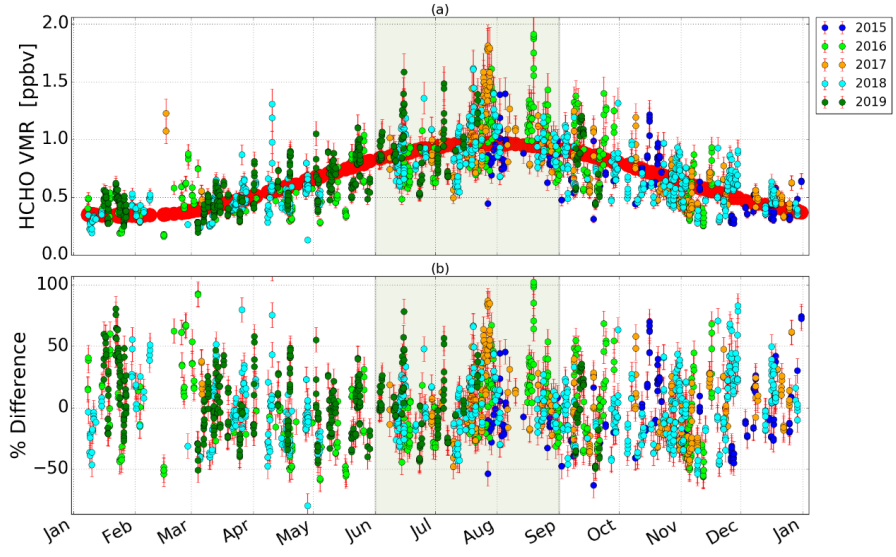

Fig. 5 (a) Seasonal variations of tropospheric HCHO VMR from 2015−2019 over eastern China. The red curve shows the seasonal mean values represented by $Y_{hcho}^{mod1}(t)$ (equation (2)). (b) Fractional differences of FTIR tropospheric HCHO VMR time series relative to their seasonal mean values . The grey vertical shaded area indicates measurements in summer (JJA).

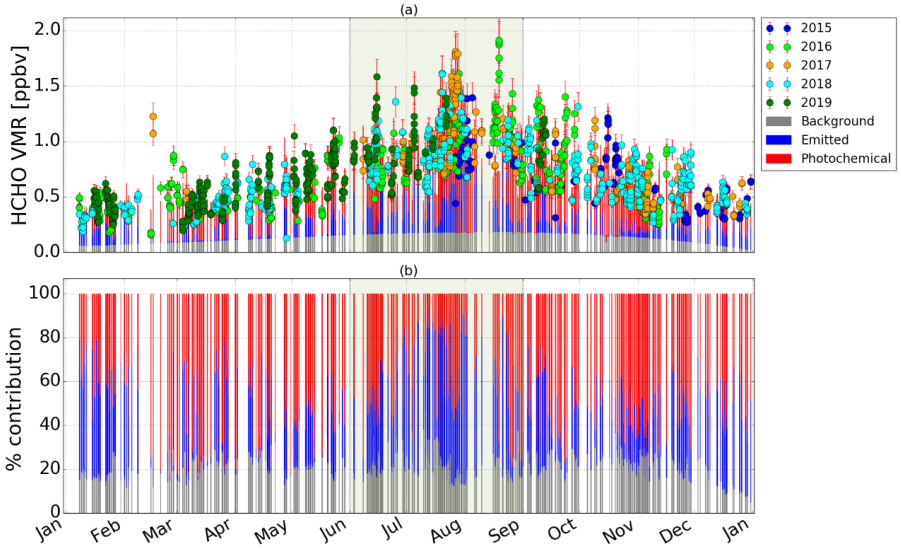

Fig. 6 (a) Separation between emitted and photochemical HCHO by using CO - O_x tracers to model FTIR observation. (b) Relative contributions of emitted, photochemical and background sources to the observed HCHO VMR from 2015−2019 over eastern China. The grey vertical shaded area indicates measurements in summer (JJA).

https://doi.org/10.5194/acp-2020-544
Preprint. Discussion started: 30 July 2020

Atmospheric Chemistry and Physics Discussions
Open Access
EGU

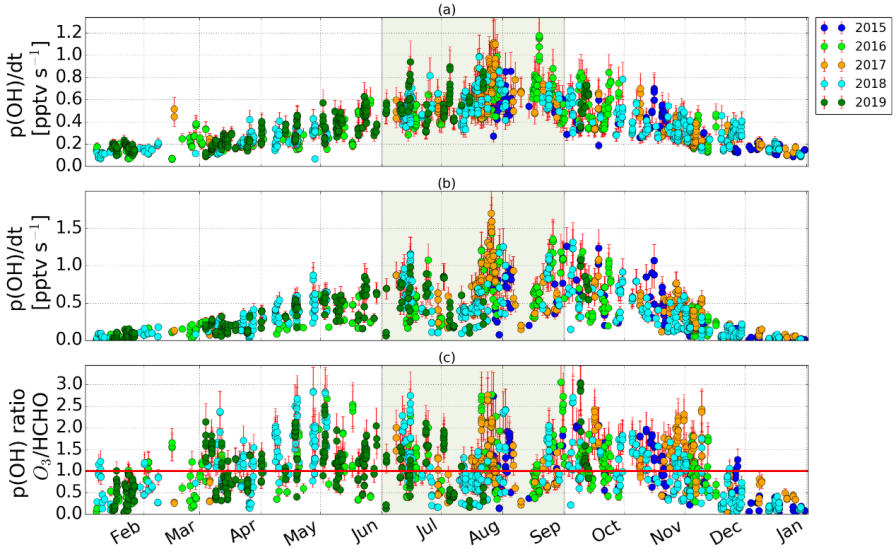

Fig. 7 Total OH radical production rates from the photolysis of HCHO (a) and O_3 (b) from 2015−2019 over eastern China. (c) The ratios of OH radical production rates from photolysis of O_3 to that from HCHO. The gray vertical shaded area indicates measurements in summer (JJA). The red line denotes one-to-one line.

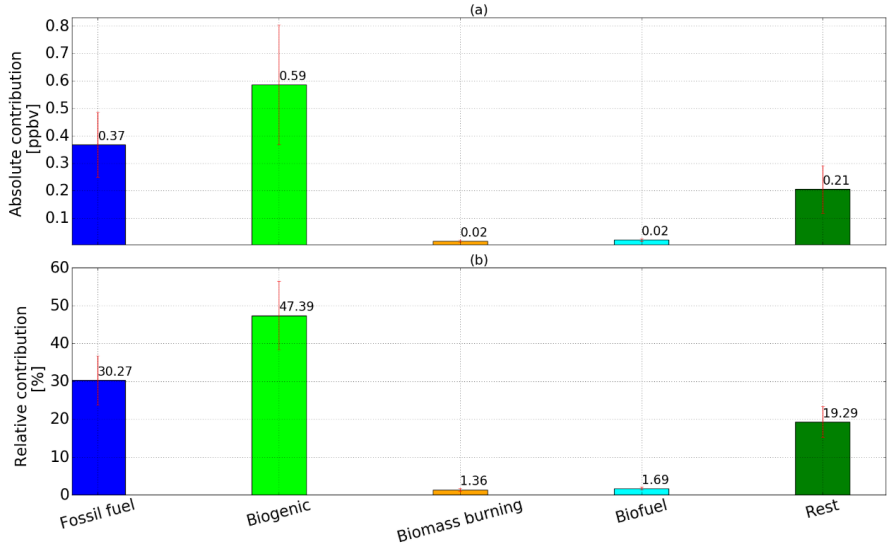

Fig. 8. Absolute (a) and relative (b) contributions of fossil fuel, biogenic, biomass burning, biofuel, and the rest emission sources to the observed HCHO summertime enhancement from 2015−2019 over eastern China. Vertical error bars represent 1-σ standard variation.

https://doi.org/10.5194/acp-2020-544
Preprint. Discussion started: 30 July 2020

Atmospheric Chemistry and Physics Discussions

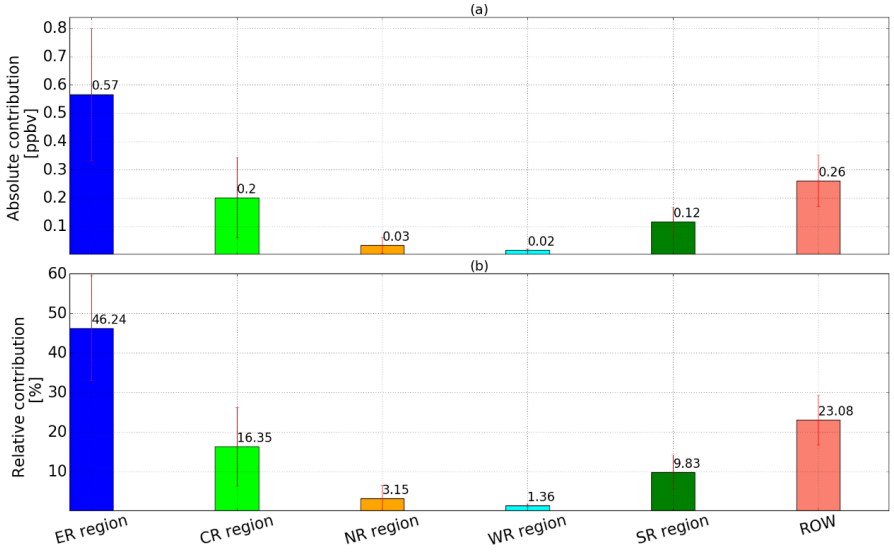

Fig. 9. Absolute (a) and relative (b) contributions of the emissions in ER, CR, NR, WR, SR, and ROW regions to the observed HCHO summertime enhancement from 2015−2019 over eastern China. Geographical definitions for these regions are summarised in Table 2. Vertical error bars represent 1-σ standard variation.